

RADIO BURSTS OBSERVED DURING SOLAR ERUPTIVE FLARES AND THEIR SCHEMATIC SUMMARY

MARIAN KARLICKÝ¹

¹*Astronomical Institute of the Academy of Sciences of the Czech Republic, CZ-25165 Ondřejov, Czech Republic*

ABSTRACT

In this review we summarize results of our analysis of the observations of solar eruptive flares made by the Ondřejov radiospectrograph for more than twenty years. We also present some Potsdam-Tremsdorf radio spectra from our common studies. Considering a 3-dimensional model of eruptive flares together with the results of our magnetohydrodynamic and particle-in-cell simulations we show an importance of decimetric radio bursts for understanding of plasma processes in eruptive flares. We present drifting pulsation structures as signatures of plasmoids, an unusual zebra pattern in the very early flare stage, narrowband dm-spikes as the bursts generated in the reconnection plasma outflows, radio bursts indicating a merging of plasmoids, pair of decimetric type III bursts indicating the electron beams propagating upwards and downwards in the solar atmosphere from the acceleration site, and a special decimetric type III burst formed probably around the plasmoid. We present unusual radio bursts connected with the rising magnetic rope at the very beginning of eruptive flares. Furthermore, based on the analysis of decimetric continua we estimated the level of the plasma turbulence in a vicinity of the flare termination shock. Interpretations of all these bursts are based on models and time coincidences with observations in X-ray, UV and optical ranges; in most cases an information about positions of these radio sources is missing. To show an importance of positional information, we present a rare example of observations, where the drifting pulsation structure was observed simultaneously with the observations made by the EOVS radio interferometer. All the presented bursts are then summarized in a new scheme of bursts and compared with the schema commonly used.

Keywords: Sun: flares – Sun: radio radiation

arXiv:2307.07144v1 [astro-ph.SR] 14 Jul 2023

1. INTRODUCTION

Solar flares are the most powerful events in the the solar system, releasing the energy up to 10^{32} erg in tens of minutes. The strongest flares are associated with coronal mass ejections and acceleration of particles into interplanetary space. From physical point of view solar flares are explosive phenomena in the solar atmosphere, in which the energy accumulated in the magnetic field and electric currents is rapidly transformed into plasma heating, plasma flows, accelerated particles and emission in a broad range of electromagnetic waves: from radio, through optical, UV, X-rays to gamma-rays. For more details, see reviews by in [Priest & Forbes \(2002\)](#); [Aschwanden \(2002\)](#); [Krucker et al. \(2008\)](#); [Schrijver \(2009\)](#); [Fletcher et al. \(2011\)](#); [Nakariakov et al. \(2016\)](#).

Generally, solar flares can be divided into eruptive flares and confined flares ([Švestka et al. 1992](#)). Note that the eruptive flares are sometimes called the LDE (long duration event) flares or two-ribbon flares. The eruptive flares belong to the most powerful classified in GOES classification as M and X flares. These flares are described by the "standard" CSHKP flare model ([Carmichael 1964](#); [Sturrock 1966](#); [Hirayama 1974](#); [Kopp & Pneuman 1976](#)), or by its generalized 3-dimensional model proposed by ([Aulanier et al. 2012](#); [Janvier et al. 2014](#)).

Because the eruptive flares influence the whole heliosphere, including the space around the Earth, these flares are of great interest for the space weather programs. They are monitored by many instruments on board of satellites and ground based observing stations in a broad range of emissions. These emissions are produced by various emission mechanisms, e.g., the bremsstrahlung for X-rays, transitions of electrons between energetic atomic levels for UV and optical emissions, gyro-synchrotron and plasma emission mechanisms for radio emission and so on. Among these mechanisms the plasma emission mechanism is special one because it is directly connected with the plasma processes in flares. Thus, solar decimetric and metric radio bursts, which are generated by this emission mechanism, give us a direct insight into flare processes. Unfortunately the bursts, especially in decimetric range, which is of high importance for diagnostics of eruptive flares, are usually only observed spectroscopically. Observations with spatial information about their sources are rare. Nevertheless, as will be shown in the following, owing to a high-time resolution of dynamical radio spectra, important results about plasma processes in solar flares can be obtained.

This review paper presents examples of the radio bursts observed in decimetric range during the eruptive flares by the Ondřejov radiospectrographs ([Jiříčka et al. 1993](#); [Jiříčka & Karlický 2008](#)). Examples were selected from numerous radio spectra recorded for more than twenty years. The paper is organized as follows: After describing a model of the eruptive flare we present a typical radio spectrum of the eruptive flare with type III and II bursts, drifting pulsation structure and high-frequency continua. Then we show unique drifting bursts in connection with the rising magnetic rope, unusual zebra pattern and slowly positively drifting bursts at the very beginning of flares. We show radio bursts connected with plasmoids, narrowband dm-spikes, a pair of normal and reverse drift type III bursts and unusual type III burst connected probably with a plasmoid. We also present the power spectral analysis of decimetric continuum and its new model. Then we show one example of the drifting pulsation structure observed simultaneously with the EOVS spatial observations. The presented bursts are interpreted within a 3-dimensional model of eruptive flares and results of numerical simulations of plasma processes in solar flares. We summarize all presented bursts into the schema which completes the "standard" schema of radio bursts in solar flares shown, e.g., in [Krueger \(1979\)](#). The paper ends with conclusions and statements expressing an importance of new instruments which would yield not only spectral, but combined spectral and spatial information about observed radio bursts.

2. MODEL OF THE ERUPTIVE FLARE

A sketch of the 3-dimensional model of the eruptive flare is shown in Figure 1. In this model the eruptive flare can be described as follows ([Priest & Forbes 2002](#); [Aschwanden 2002](#); [Krucker et al. 2008](#); [Schrijver 2009](#); [Fletcher et al. 2011](#); [Nakariakov et al. 2016](#); [Aulanier et al. 2012](#); [Janvier et al. 2014](#)):

First, along the neutral line between magnetic polarities in the active region, a magnetic rope (i.e. current-carrying loop) is formed owing to shear and vortex plasma flows at the photospheric level. At its bottom part a cold and dense plasma condensates into the filament, which is dark in contrast to the surrounding bright chromosphere. Then this magnetic rope together with the filament becomes unstable due to torus or kink instabilities or external perturbations (particle beams, waves or shocks) ([Kliem & Török 2006](#); [Kliem et al. 2010](#); [Karlický & Jungwirth 1989](#); [Odstrčil & Karlický 1997](#)). Another possibility is that the upper part of the magnetic rope interacts with the above-lying magnetic field lines and through magnetic reconnection a stabilizing magnetic force decreases ([Aurass et al. 2011](#)). As a result of all the mentioned processes the magnetic rope moves upwards, but its ends are still anchored in dense layers of the solar atmosphere, forming thus a growing current-carrying loop. Although an enormous electric

current can flow through this magnetic rope (up to 10^{12} A), this current does not dissipate here, because the electric current density is low. The situation is different below the rising rope, where the current sheet is formed step by step (Yan et al. 2018). It is assumed that when this current sheet becomes sufficiently narrow and the current density inside this sheet sufficiently high, then the plasmoid instability starts and magnetic reconnection follows (Huang et al. 2017). A plasma together with magnetic field lines is sucked from both sides of the current sheet into the X-point region and accelerated to the Alfvén speed in vertical (upward and downward) plasma outflows. The upward oriented outflow even accelerates the rising magnetic rope, while the downward oriented outflow is stopped above the flare loop arcade, where the so called termination shock can be formed (Aurass & Mann 2004). At the X-point within the magnetic reconnection region a strong electric field is generated, which accelerates electrons and ions to high energies (Karlický 2008; Dahlin et al. 2014). These particles propagate along the magnetic field lines. Some of them propagate upwards in the solar atmosphere, generating radio emission by the plasma emission mechanism, e.g. type III radio bursts (Suzuki & Dulk 1985). The electrons propagating downwards generate radio continua (at frequencies above about ~ 2 GHz) by the gyro-synchrotron mechanism (Krueger 1979) and the hard X-ray emission by bremsstrahlung (Brown 1971). Simultaneously, electrons in the whole flare generate various fine structures in the radio spectrum via the plasma emission mechanisms (Chernov 2011). The superthermal ions, especially protons, propagating downwards are sources of gamma-rays (Akimov et al. 1996). During the magnetic reconnection process the flare plasma is strongly heated, which leads to an increase of the soft X-ray emission. The whole magnetic flare structure expands in the process called coronal mass ejection (CME) and magnetohydrodynamic shocks are produced. Such shocks then generate type II radio bursts (Nelson & Melrose 1985). Furthermore, associated waves propagate along the solar surface as Moreton and EIT (UV) waves (Moreton 1960; Thompson et al. 1998). During some flares even large amplitude loop oscillations and seismic waves have been detected (Nakariakov et al. 2016; Kosovichev & Zharkova 1998).

3. EXAMPLES OF RADIO BURSTS AND THEIR INTERPRETATIONS

In the following we present examples of radio bursts observed during eruptive flares. They are interpreted based on the 3-dimensional model of eruptive flares and corresponding numerical simulations.

3.1. *Radio bursts observed during the 12 April 2001 flare*

Figure 2A shows a typical radio spectrum of the eruptive flare. This spectrum was recorded during the 12 April 2001 flare, classified as X2.0 flare which started at 09:39 UT and ended at 10:49 UT. At frequencies above about 3 GHz this spectrum shows the continuum emission (type IV radio burst), which is believed to be generated by the gyro-synchrotron emission mechanism. On the other hand, below 3 GHz the observed bursts are produced by the plasma emission mechanism due to their fine structures. In this case, the square of their frequency is proportional to the electron plasma density in their sources. Because the solar atmosphere is gravitationally stratified, i.e., the plasma density decreases increasing the height in the solar atmosphere, a frequency distribution of bursts in this spectrum roughly corresponds to the distribution of their sources in heights. Thus, we can see that type III bursts, observed as rapidly drifting in the 0.04 – 0.3 GHz range at about 10:17 – 10:20 UT and generated by electron beams (propagating into the upper corona), are at higher altitude than that of the drifting pulsating structure (DPS) observed at 10:14:30 – 10:22:00 UT in the 0.45 – 2.0 GHz range. Furthermore, the spectrum shows two branches of type II radio burst observed at 10:15 – 10:23 UT in the 0.04 – 0.6 GHz range and generated by the flare shock. To show correspondence of these bursts with the 3-D model of the eruptive flare, in Figure 2B a model scenario is shown. The rising magnetic rope (the uppermost plasmoid) generates underneath a vertical current sheet, where secondary plasmoids and flare loop are generated due to the plasmoid instability. Above the magnetic rope the shock is produced owing to its super-alfvenic velocity. While the high frequency continuum is generated at the bottom part of this structure, at flare loops, shock generates type II burst on fundamental and harmonic plasma frequency. Electrons are accelerated at X-magnetic field points located between plasmoids. Some electrons escape from this structure and generate type III bursts, Other accelerated electrons are trapped in the plasmoid of the magnetic rope or in secondary plasmoids. Here, the electrons generate the plasma waves that are then transformed to the electromagnetic (radio) waves observed as DPSs. The density in the plasmoid is in some range, which thus corresponds to the bandwidth of DPS. The plasmoids move upwards or downwards along the flare current sheet with velocities that are smaller than local Alfvén speed. In the radio spectrum the plasmoid motion is expressed by the frequency drift of DPS. Pulses in DPS are owing to a quasi-periodic regime of the electron acceleration. For more details about the drifting pulsation structure and its model, see Kliem et al. (2000); Bárta et al. (2008a). As concerns to more details about this radio event, see Mészárosová et al. (2006).

3.2. Radio burst observed at the beginning of the 24 September 2001 flare

At the very beginning of the 24 September 2001 flare (X2.6, start 09:20 UT and end 11:39 UT), just before a series of type III bursts (starting at 10:18 UT and indicating the flare impulsive phase), a very unusual burst was observed at 09:30 – 10:18 in the 800 – 40 MHz range (Figure 3). It happened in the phase when the magnetic loop rises (Fárník et al. 2003). Therefore, we call this burst as the rope rising continuum. It looks as some continuum superimposed by some weak type I-like bursts. Its starting boundary drifts from higher to lower frequencies. Assuming the plasma emission mechanism of this burst and the emission on the fundamental frequency then the frequency drift of this burst in the model of the solar atmosphere (Aschwanden 2002) corresponds to the upwards velocity 280 km s^{-1} . This velocity is in the range of the velocities of rising magnetic rope, therefore we think that this burst is generated on the outer boundary of the rising rope, where the rope interacts with the above-lying magnetic field or inside the rope due to some inner-rope magnetic reconnection. Moreover, we think that type III bursts started just when below the rising magnetic rope a sufficiently narrow current sheet is formed and the flare magnetic reconnection starts. Such a burst is very rare. We found a similar burst only at the very beginning of the 7 June 2011 flare (Karlický et al. 2020b).

3.3. Radio bursts observed at the beginning of the 6 September 2017 flare

The 6 September 2017 flare was classified as X9.3 with its start at 11:53 UT and end at 12:10 UT. The flare was so strong that the impact of its radio emission has been found at the frequency 1.2 GHz of Global Navigation Satellite System (Sato et al. 2018). For more details about this flare, see Mitra et al. (2018) and references therein. The radio spectrum at the beginning of this flare is shown in Figure 4A. As seen here, the whole radio emission is rapidly drifting to lower frequencies. The most remarkable aspect of this radio burst is the zebra-like structure observed at the starting boundary of this globally drifting burst (Figure 4B). Owing to the flare phase of its observation and relatively broadband zebra stripes it differs from normal zebras that are usually observed in later flare phases. Although we cannot exclude that this zebra-like structure is generated by some of mechanisms considered for normal zebras (Chernov 2011), we propose that at this flare phase the zebra-like structure can be the radio emission from four plasmoids distributed in the vertical flare current sheet. If so then the emission mechanism generating this zebra-like structure would be the same as in DPSs (Kliem et al. 2000).

3.4. Slowly positively drifting bursts observed in the 2 April 2022 flare

Figure 5 upper part shows the radio spectrum observed at the very beginning of the eruptive flare, where two slowly positively drifting bursts (1 and 2) can be seen. Their frequency drift is about 100 MHz s^{-1} . At the same time the AIA/SDO image (Figure 5 bottom part) shows a bright helical structure (HS) as a part of the rising magnetic rope. In accordance with Zemanová et al. (2020) we interpret these slowly positively drifting bursts as generated by the particle beams propagating in the bright helical structure. Owing to their propagation along the helical trajectory, that is even deflected from the vertical direction in the gravitationally stratified atmosphere, the frequency drift of these bursts is much smaller compared with the typical frequency drift of the reverse type III bursts in this frequency range ($\sim 1 \text{ GHz s}^{-1}$). This interpretation is supported by a brightening (B) at the location, where the magnetic rope is anchored. The bright helical structure as well as slowly positively drifting bursts show a flaring activity in the rising magnetic rope. Note, that such an activity is not considered in the standard CSHKP flare model.

3.5. Drifting pulsation structure observed during the 18 August 1998 flare

Drifting pulsation structures are commonly observed at the very beginning of the eruptive flares in the decimetric range. One example is shown in Figure 6A that was observed during the X2.8 flare, which started at 08:18 UT and ended at 08:45 UT (Karlický et al. 2002). As seen in this spectrum the frequency drift of DPS varies in time. But globally, the drift is from higher to lower frequencies as in the most DPS cases. In agreement with the interpretation of DPS in the paper by Kliem et al. (2000) we interpret the drift variation by a change of the propagation direction of the emitting plasmoid along the vertical flare current sheet and the global drift as an upwards motion of the plasmoid. To support this interpretation we made numerical simulations showing the upwards motion of the plasmoid in the current sheet, see different evolution phases of the plasmoid in Figure 6B. For more details about these numerical simulations, see the paper by Bárta et al. (2008b).

3.6. Drifting pulsation structures and narrowband dm-spikes observed during the 28 March 2001 flare

The numerical simulations presented in [Bárta et al. \(2008b\)](#) also show that the plasmoid can move downwards along the flare current sheet and interacts with the underlying flare arcade (Figure 7C). Therefore, we searched for appropriate bursts and we found the radio spectrum of the 28 March 2001 flare (M4.3, start 12:08 UT and end 12:15 UT ([Mészárosová et al. 2003](#))), see Figure 7A. Here, there are two DPSs with the positive frequency drift that are followed by a cloud of the narrowband dm-spikes on higher frequencies. To explain processes in these bursts a scenario is added in Figure 7B. Here, the plasmoids emitting DPSs move downwards as in the numerical simulation and then they interact with the flare arcade. In the papers by [Karlický et al. \(1996, 2000\)](#) we found that the Fourier spectra of the narrowband spikes are the power-law and their power-law indices are close to the power-law index of the Kolmogorov spectra ($-5/3$). Based on this finding we propose that during the interaction of plasmoids with the flare arcade the plasmoids are fragmented. Thus, they form a cascade of fragmented plasmoids, where each plasmoid emits as DPS. Because a cascade of the fragmented plasmoids consists the plasmoids of different sizes then as a result we observe a cloud of dm-spikes having different frequency bandwidths.

3.7. Radio bursts observed during the 28 September 2001 flare

In the flare current sheet two or even more plasmoids can be formed and merge into a larger plasmoid (Figure 8B) ([Bárta et al. 2008b](#)). The merging process generates oscillations of the resulting plasmoid ([Tajima et al. 1987](#)). As presented in Figures 3-5 in the paper by ([Karlický 2017](#)) oscillations of the merging plasmoid causes oscillations of the radio emission frequency. Considering the results of all these simulations we think that the radio bursts in Figure 8A corresponds to these processes. On the spectrum, at 08:39 - 08:42 UT we can see several DPSs that changed after 08:42 UT into one DPS oscillating in the frequency. This spectrum was observed during the flare starting at 08:10 UT and ending at 08:50 UT.

3.8. Type III bursts observed during the 26 September 2011 and 12 February 2010 flares

Type III bursts are quite common in any solar flares. However, in some flares special type III bursts are observed. Figure 9 shows two examples of special type III bursts. In the upper part of this figure pairs of type III bursts with the normal and reverse (RS) drift are show. This example was observed during the 26 September 2011 flare (start at 06:21 UT and end at 06:30 UT). The GOES soft X-ray classification is unknown, but during this flare the hard X-ray emission was observed ([Tan et al. \(2016\)](#)). These pairs of type III bursts are explained by the electron beams, accelerated at the X-point of magnetic reconnection. One beam is propagating upwards (normal type III burst) and the second one downwards, generating thus the reverse drifting type III burst. The second example, presented in Figure 9B, is a unique type III burst with some hole inside. This special type III burst was observed during the M9.2 flare (start at 11:25 UT and end 11:32 UT), for more details about this flare, see [Chernov et al. \(2014\)](#). We propose that in this case the electron beam accelerated at the X-point of the magnetic reconnection moves around the plasmoid. To explain the processes generating the both examples of type III bursts a scenario of assumed processes is shown in Figure 9C.

3.9. Decimetric continuum observed during the later phase of the 25 June 2015 flare

Figure 10 upper part shows the radio spectrum with the decimetric continuum observed in the 25 June 2015 flare. In the 09:11-09:24 time interval we expressed frequency variations of the high-frequency continuum boundary (Figure 10 bottom part A). Its corresponding power spectrum is in B. Then we selected the radio flux variations at the frequency in the range of the continuum boundary variations (C) (at 1478 MHz) and computed its power spectrum (D). The power-law index in the both cases is close to the Kolmogorov turbulence index $-5/3$ that indicates the turbulence in the decimetric continuum source.

The continuum was observed after the flare impulsive phase when the X-ray flare emission according to GOES X-ray curves was still enhanced. Therefore, at this flare phase, in agreement in the standard flare model, we propose the following explanation of the presented results, see the schema of the dm-continuum source in Figure 10. The plasma outflow from the reconnection site is in a turbulent state. Owing to this outflow, in front of the flare loop the termination shock is formed ([Warmuth et al. 2009](#)). The outflow carries the plasma with the magnetic field to the termination shock. Here, electrons are accelerated by adiabatic reflection in a quasi-perpendicular shock. This is known as fast-Fermi acceleration or shock drift acceleration ([Holman & Pesses 1983](#); [Krauss-Varban & Wu 1989](#); [Vandas & Karlický 2011](#)). Because the plasma entering the termination shock is in the turbulent state, its magnetic field changes direction and, therefore, an efficiency of the acceleration is changed as shown by simulations made by

Guo & Giacalone (2010). Thus, at the termination shock spatial-spectral properties of the turbulent plasma outflow are transformed into time-spectral properties of accelerated electron beams. Then these beams propagate upstream or downstream of the termination shock and generate radio emission by the plasma emission mechanism similarly as in the case of herringbones in the type II bursts. Owing to a high density gradient in the region of continuum generation the frequency drift of the beam emission is much higher than in the herringbones case. It is so high that it is not measurable by the used time resolution of radio spectra. For more details, see Karlický (2023).

3.10. *Drifting pulsation structure observed during the 10 September 2017 flare together with the EOVSAs spatial observation*

Positional observations of solar radio bursts in decimetric range, which are important for the understanding of flare core processes, are not regular. Nevertheless, new instruments like Expanded Owens Valley Solar Array (EOVSA) (Gary et al. 2013), Chinese Spectral Radio Heliograph (Li et al. 2012) and Brazilian Decimetre Array (Ramesh et al. 2007) started observations. To show that combined positional and spectral observations are very important, in Figure 11A we show observations of DPS from the X8.2 flare (start at 15:35 UT and end 16:39 UT) simultaneously with EOVSAs observations (Figure 11B). Although the frequency range of EOVSAs observations at this day does not cover the frequency range of DPS, the observations are very interesting. Namely, Figure 11 shows that the start and two band structure of DPS coincided with a tearing of the ejected filament seen by SDO/AIA 193 Å observations. At the same time EOVSA shows a prolongation of sources, especially on the lowest frequencies (~ 3.5 GHz). Because later at space of the filament tearing the flare current sheet was formed (Yan et al. 2018) we interpret these observations as follows: When the filament starts to be teared the current sheet is formed. Inside this sheet the magnetic reconnection starts, accelerating electrons which are trapped at ends of the broken filament. Thus, these electrons at these filament ends, having different densities, generate two bands of DPS. For more details, see Karlický et al. (2020a).

3.11. *Schema of bursts based on the presented radio spectra*

Considering the frequency range and times of all the presented bursts we summarize them into the schema shown in Figure 12A. This schema is valid for the eruptive flares, especially at their beginnings and in the decimetric range. While the rope rising continuum, slowly positively drifting bursts and special type III burst formed around the plasmoid are very rare, others like DPSs, type III and II bursts, and decimetric continuum are frequent. For statistical analysis of DPSs and other bursts in the decimetric range, see Jiříčka et al. (2001). The schema starts with the rope rising continuum or slowly positively drifting bursts, which in many spectra of the eruptive flares are missing. In most cases the eruptive flares start with DPS in the decimetric range (Nishizuka et al. 2015). They drift usually towards lower frequencies. DPS with the positive frequency drift and narrowband dm-spikes are less frequent. Practically in all eruptive flares we can observe dm- and m-type III bursts that are in many cases followed by decimetric continua and type II burst at frequencies in the metric range. For comparison, in Figure 12B we added the "standard" schema of radio bursts in solar flares (Krueger 1979). Comparing both the schemas we can see that in the new scheme there are new and rarely observed bursts, that complete the "standard" schema.

4. CONCLUSIONS

We presented examples of some typical and also unusual bursts that were interpreted using the 3-dimensional model of the eruptive flares and corresponding numerical simulations. We showed the unusual rope rising continuum which is associated with the rising magnetic rope at the beginning of the flare. We also presented slowly positively drifting bursts observed simultaneously with the bright helical structure inside the rising magnetic rope. It shows flaring processes in this rope that are not considered in the standard CSHKP model of the eruptive flares. Namely, in the standard flare model it is assumed that in the magnetic rope there is a huge electric current, but its density, which high values are essential for any flaring activity, is very low due to a large cross-section of the magnetic rope. The primary energy-release process in the standard flare model is the magnetic reconnection at the location below the rising magnetic rope.

Typical drifting pulsation structures were presented as signatures of plasmoids; those with the negative or positive frequency drift as the emission from the plasmoid moving upwards or downwards in the solar atmosphere. The radio spectrum corresponding to merging of two plasmoids was also shown. Maybe that also the unusual zebra, observed at the very early stage of the flare, can be explained as the emission from the plasmoids distributed in the vertical flare current sheet.

We also presented the narrowband dm-spikes as a result of the fragmented magnetic reconnection, a pair of the decimetric type III bursts showing the electron beams propagating from the acceleration site upwards and downwards in the solar atmosphere, and an unusual decimetric type III burst probably formed by the electron beam propagating around the plasmoid. We interpreted decimetric continua as a radio emission of electron beams accelerated at the termination shock formed by a turbulent reconnection plasma outflow above flare loops.

We summarized these bursts into a new schema of radio bursts which complete the previous schema of the radio bursts in solar flares, especially for the eruptive flares at their beginnings. We showed an importance of observations in the decimetric range for understanding of the flare processes at the early stages of eruptive flares. We also presented one example of simultaneous observations of the drifting pulsation structure together with the positional observation made by the EOVSA radiointerferometer. However, the observations of radio source positions in the decimetric range are rare. The example with positional observations clearly shows how such combined spectral and positional observations are important. Therefore, new solar-dedicated radio facilities, working in the decimetric range, like the project of Frequency Agile Solar Radiotelescope (FASR) that is planned to be an extension of EOVSA radiointerferometer, are highly desirable.

We acknowledge support from the project RVO-67985815 and Grant 22-34841S of the Grant Agency of the Czech Republic.

REFERENCES

- Akimov, V. V., Ambrož, P., Belov, A. V., et al. 1996, *SoPh*, 166, 107
- Aschwanden, M. J. 2002, *SSRv*, 101, 1
- Aulanier, G., Janvier, M., & Schmieder, B. 2012, *A&A*, 543, A110
- Aurass, H. & Mann, G. 2004, *ApJ*, 615, 526
- Aurass, H., Mann, G., Zlobec, P., & Karlický, M. 2011, *ApJ*, 730, 57
- Bárta, M., Karlický, M., & Žemlička, R. 2008a, *SoPh*, 253, 173
- Bárta, M., Vršnak, B., & Karlický, M. 2008b, *A&A*, 477, 649
- Brown, J. C. 1971, *SoPh*, 18, 489
- Carmichael, H. 1964, *NASA Special Publication*, 50, 451
- Chernov, G. 2011, *Fine Structure of Solar Radio Bursts*, Berlin: Springer
- Chernov, G. P., Fomichev, V. V., Gorgutsa, R. V., et al. 2014, *Geomagnetism and Aeronomy*, 54, 406
- Dahlin, J. T., Drake, J. F., & Swisdak, M. 2014, *Physics of Plasmas*, 21, 092304
- Fárník, F., Hudson, H. S., Karlický, M., & Kosugi, T. 2003, *A&A*, 399, 1159
- Fletcher, L., Dennis, B. R., Hudson, H. S., et al. 2011, *SSRv*, 159, 19
- Gary, D. E., Fleishman, G. D., & Nita, G. M. 2013, *SoPh*, 288, 549
- Guo, F. & Giacalone, J. 2010, *ApJ*, 715, 406
- Hirayama, T. 1974, *SoPh*, 34, 323
- Holman, G. D. & Pesses, M. E. 1983, *ApJ*, 267, 837
- Huang, Y.-M., Comisso, L., & Bhattacharjee, A. 2017, *ApJ*, 849, 75
- Janvier, M., Aulanier, G., Bommier, V., et al. 2014, *ApJ*, 788, 60
- Jiříčka, K. & Karlický, M. 2008, *SoPh*, 253, 95
- Jiříčka, K., Karlický, M., Mészáros, H., & Snížek, V. 2001, *A&A*, 375, 243
- Jiříčka, K., Karlický, M., Kepka, O., & Tlamicha, A. 1993, *SoPh*, 147, 203
- Karlický, M. 2008, *ApJ*, 674, 1211
- Karlický, M. 2017, *A&A*, 602, A122
- Karlický, M. 2023, *SoPh*, accepted
- Karlický, M., Chen, B., Gary, D. E., Kašparová, J., & Rybák, J. 2020a, *ApJ*, 889, 72
- Karlický, M., Fárník, F., & Mészáros, H. 2002, *A&A*, 395, 677
- Karlický, M., Jiříčka, K., & Sobotka, M. 2000, *SoPh*, 195, 165
- Karlický, M. & Jungwirth, K. 1989, *SoPh*, 124, 319
- Karlický, M., Kašparová, J., & Sych, R. 2020b, *ApJ*, 888, 18
- Karlický, M., Sobotka, M., & Jiříčka, K. 1996, *SoPh*, 168, 375
- Kliem, B., Karlický, M., & Benz, A. O. 2000, *A&A*, 360, 715
- Kliem, B., Linton, M. G., Török, T., & Karlický, M. 2010, *SoPh*, 266, 91
- Kliem, B. & Török, T. 2006, *PhRvL*, 96, 255002
- Kopp, R. A. & Pneuman, G. W. 1976, *SoPh*, 50, 85
- Kosovichev, A. G. & Zharkova, V. V. 1998, *Nature*, 393, 317

- Krauss-Varban, D. & Wu, C. S. 1989, *J. Geophys. Res.*, 94, 15367
- Krucker, S., Battaglia, M., Cargill, P. J., et al. 2008, *A&A Rv*, 16, 155
- Krueger, A. 1979, *Introduction to solar radio astronomy and radio physics*, Geophysics and Astrophysics Monographs, Dordrecht: Reidel, 1979, p.115
- Li, S., Yan, Y., Wang, W., & Liu, D. 2012, *IAU Special Session*, 6, E5.06
- Mészárosová, H., Karlický, M., Rybák, J., Fárnik, F., & Jiříčka, K. 2006, *A&A*, 460, 865
- Mészárosová, H., Veronig, A., Zlobec, P., & Karlický, M. 2003, *A&A*, 407, 1115
- Mitra, P. K., Joshi, B., Prasad, A., Veronig, A. M., & Bhattacharyya, R. 2018, *ApJ*, 869, 69
- Moreton, G. E. 1960, *AJ*, 65, 494
- Nakariakov, V. M., Pilipenko, V., Heilig, B., et al. 2016, *SSRv*, 200, 75
- Nelson, G. J. & Melrose, D. B. 1985, *Type II bursts.*, ed. D. J. McLean & N. R. Labrum, 333–359
- Nishizuka, N., Karlický, M., Janvier, M., & Bárta, M. 2015, *ApJ*, 799, 126
- Odstrčil, D. & Karlický, M. 1997, *A&A*, 326, 1252
- Priest, E. R. & Forbes, T. G. 2002, *A&A Rv*, 10, 313
- Ramesh, R., Sawant, H. S., Cecatto, J. R., et al. 2007, *Advances in Space Research*, 39, 1451
- Sato, H., Jakowski, N., Berdermann, J., Jiříčka, K., & Heßelbarth, A. 2018, in *AGU Fall Meeting Abstracts*, Vol. 2018, SA34A–04
- Schrijver, C. J. 2009, *Advances in Space Research*, 43, 739
- Sturrock, P. A. 1966, *Nature*, 211, 695
- Suzuki, S. & Dulk, G. A. 1985, *Bursts of type III and type V.*, ed. D. J. McLean & N. R. Labrum, 289–332
- Švestka, Z., Jackson, B. V., & Machado, M. E., eds. 1992, *Lecture Notes in Physics*, Berlin Springer Verlag, Vol. 399, *Eruptive Solar Flares*
- Tajima, T., Sakai, J., Nakajima, H., et al. 1987, *ApJ*, 321, 1031
- Tan, B. L., Karlický, M., Mészárosová, H., et al. 2016, *SoPh*, 291, 2407
- Thompson, B. J., Plunkett, S. P., Gurman, J. B., et al. 1998, *Geophys. Res. Lett.*, 25, 2465
- Vandas, M. & Karlický, M. 2011, *A&A*, 531, A55
- Warmuth, A., Mann, G., & Aurass, H. 2009, *A&A*, 494, 677
- Yan, X. L., Yang, L. H., Xue, Z. K., et al. 2018, *ApJL*, 853, L18
- Zemanová, A., Karlický, M., Kašparová, J., & Dudík, J. 2020, *ApJ*, 905, 111

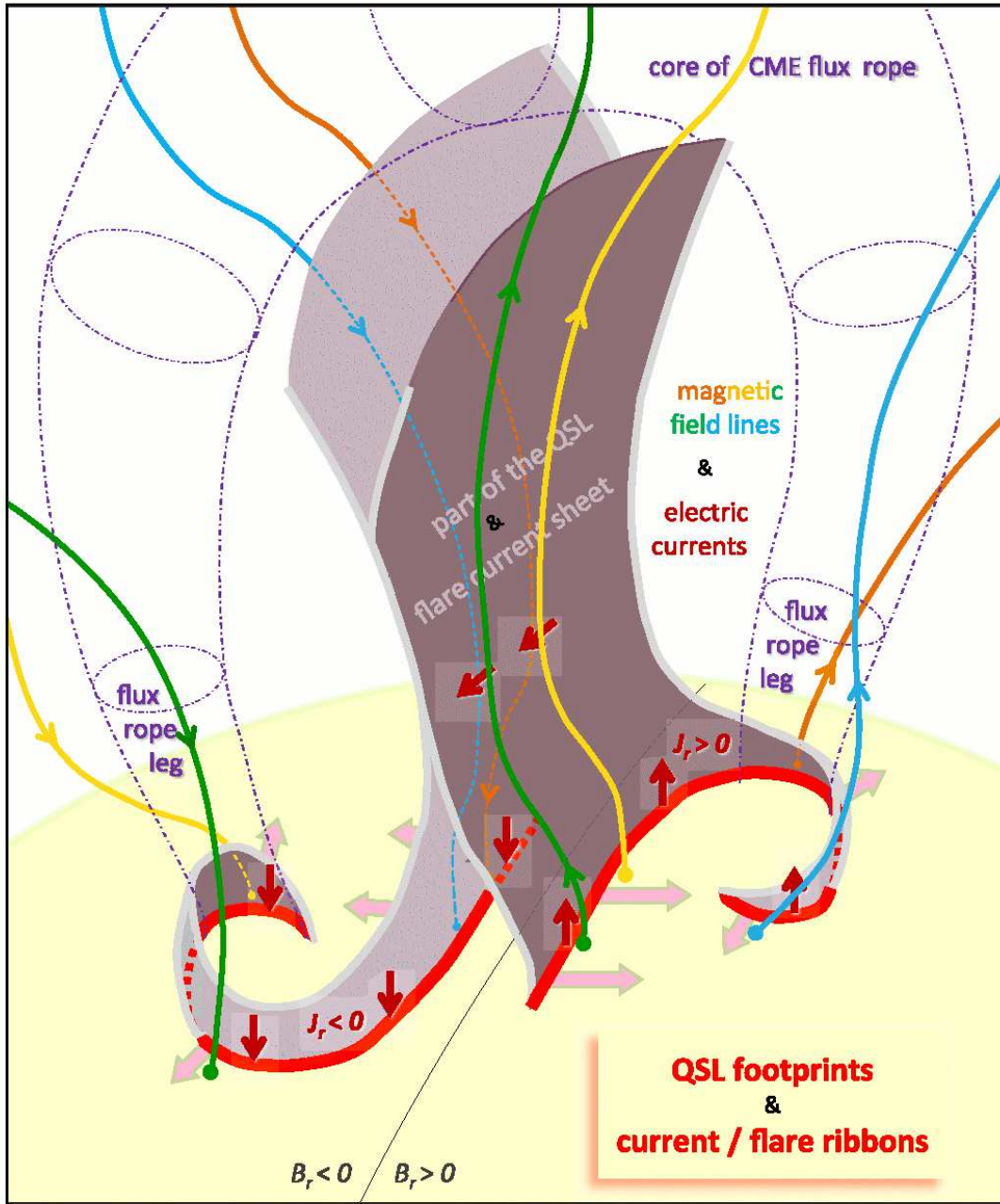


Figure 1. The 3D model of eruptive solar flares (Janvier et al. 2014).

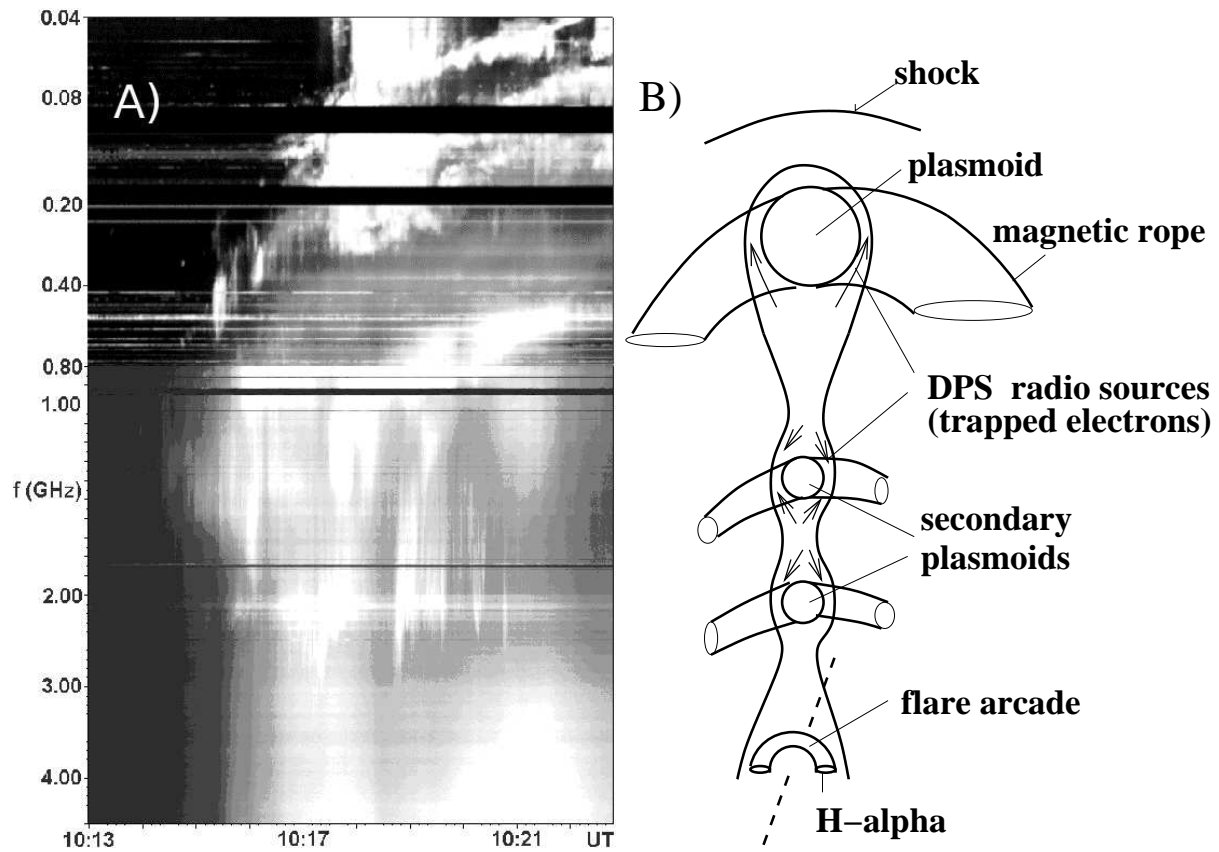


Figure 2. A) The 0.04–4.5 GHz radio spectrum observed during the 12 April 2001 flare by the Potsdam-Tremsdorf (0.04–0.8 GHz range) and the Ondřejov radiospectrographs (0.8–4.5 GHz), showing the drifting pulsating structure (DPS) at 10:17:20 – 10:22:00 UT in the 0.45–1.5 GHz range and the type II radio burst (generated by a shock wave) at 10:17 – 10:33 UT in the 0.04–0.3 GHz range. B) Flare scenario: The rising magnetic rope (the uppermost plasmoid) generates underneath a vertical current sheet, where further plasmoids (producing DPSs) are generated due to the tearing-mode instability. Above this main rope, the shock, producing type II radio burst, is generated; compare this scenario with the radio spectrum in the left part of the figure.

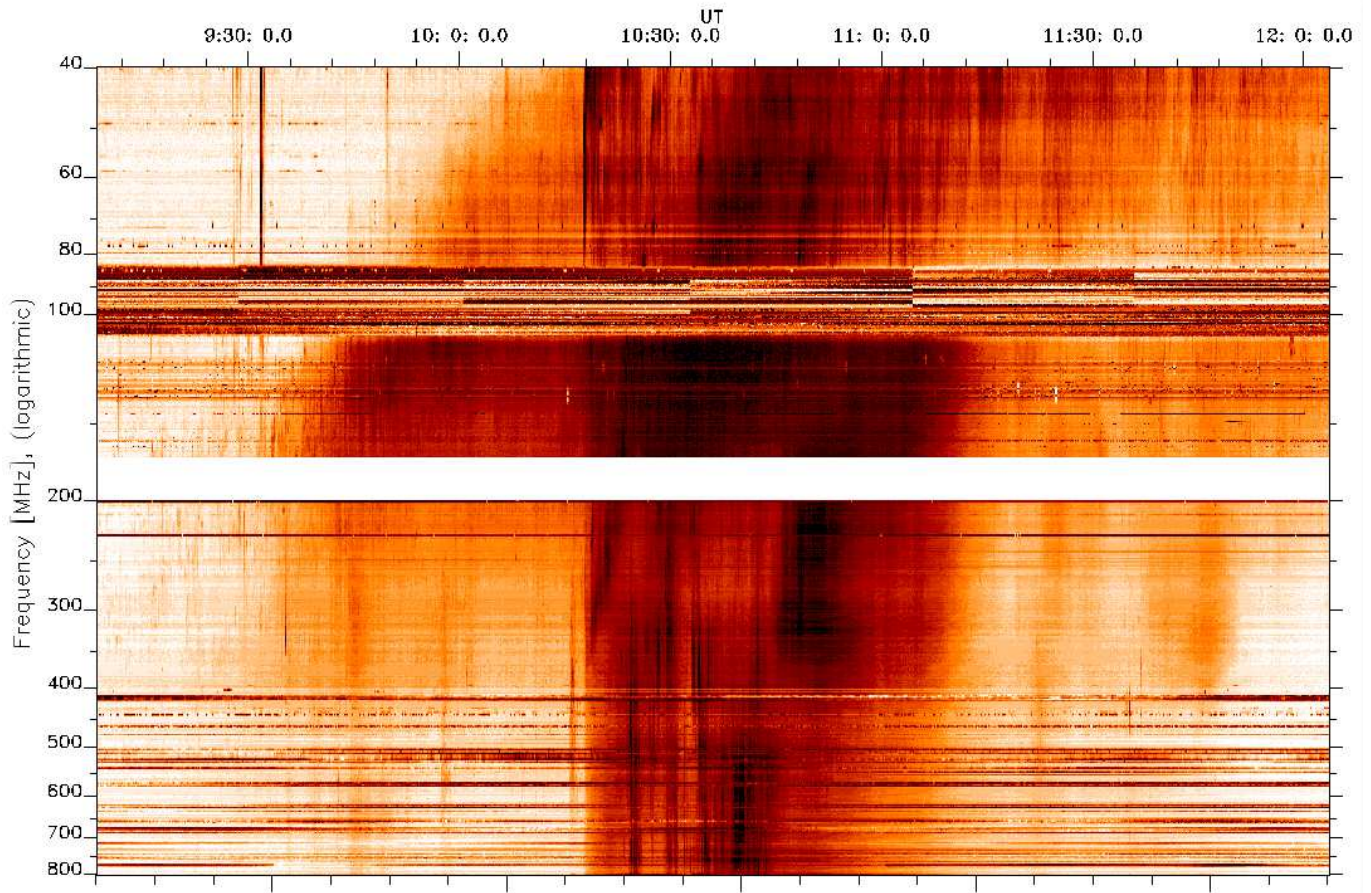


Figure 3. The 40-800 MHz Potsdam-Tremsdorf radio spectrum observed at 09:00-12:00 UT on September 24, 2001 (courtesy Dr. A. Klassen).

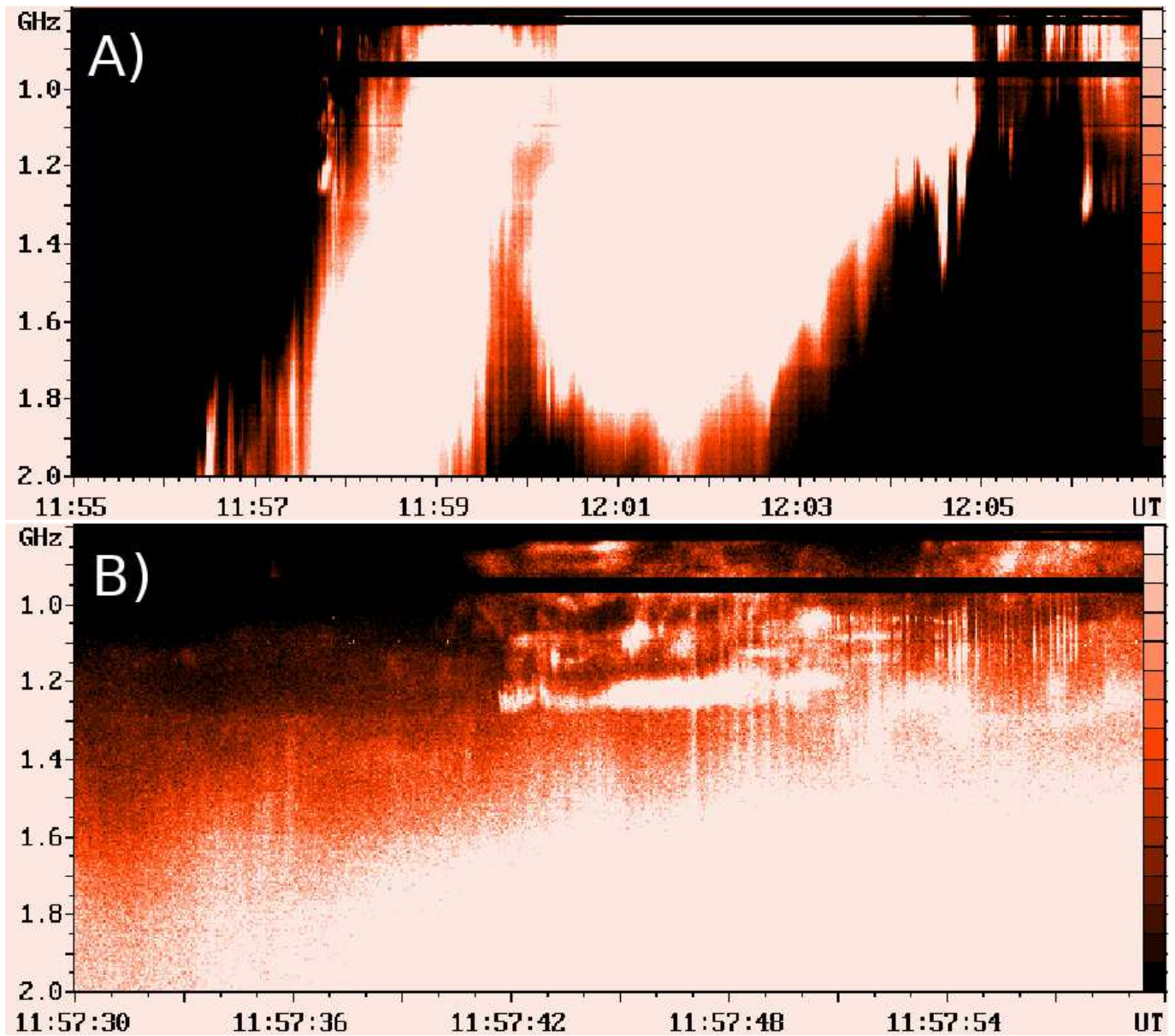


Figure 4. A) Radio spectrum of the 6 September 2017 flare observed by the Ondřejov radiospectrograph. B) The detail showing an unusual zebra-like burst.

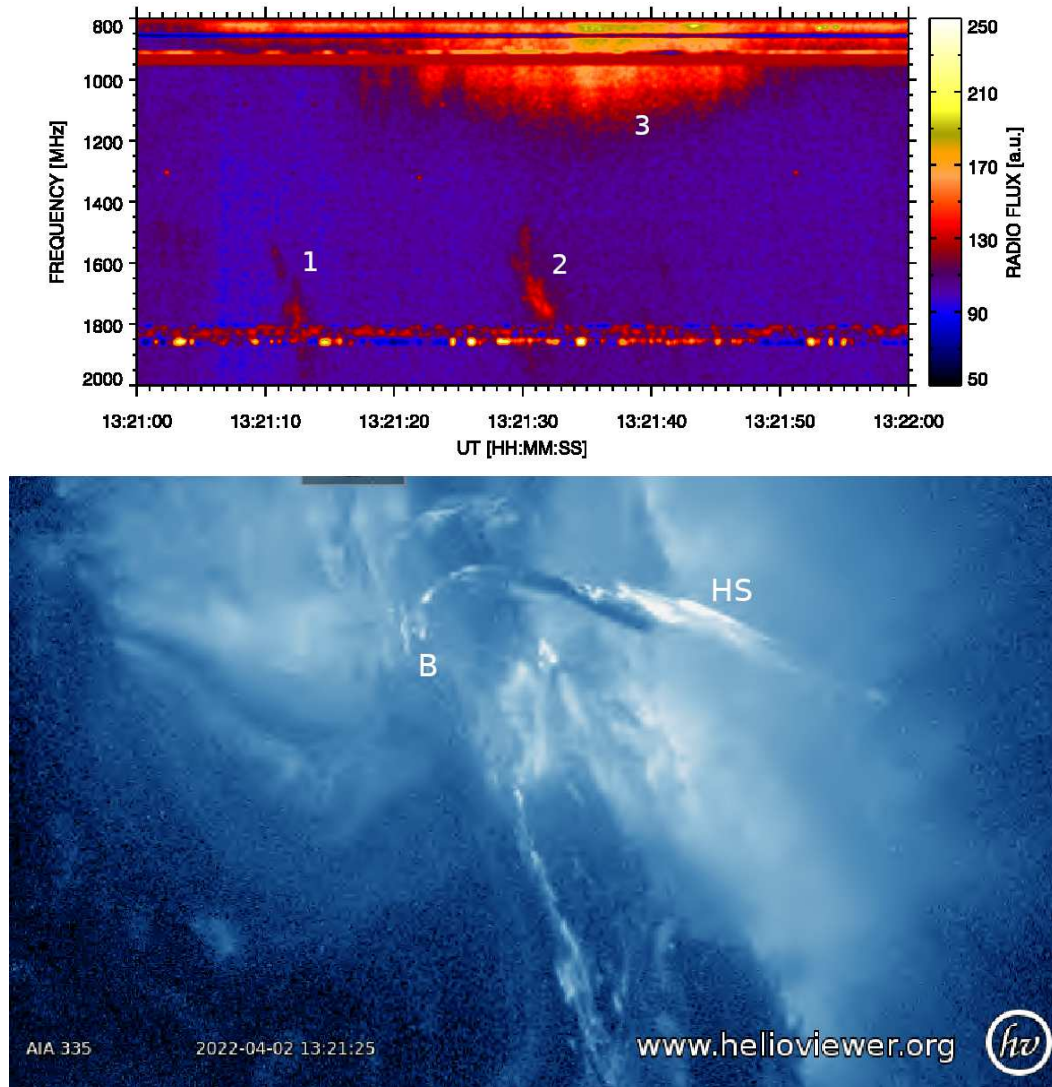


Figure 5. Upper: Radio spectrum at the very beginning of the 2 April 2022 flare with the slowly positively drifting bursts (1 and 2), 3 means continuum. Bottom: The associated AIA/SDO 335 Å image, observed at 13:21:25 UT, showing a bright helical structure (HS) inside the rising magnetic rope. B means the brightening at the footpoint of the rising magnetic rope.

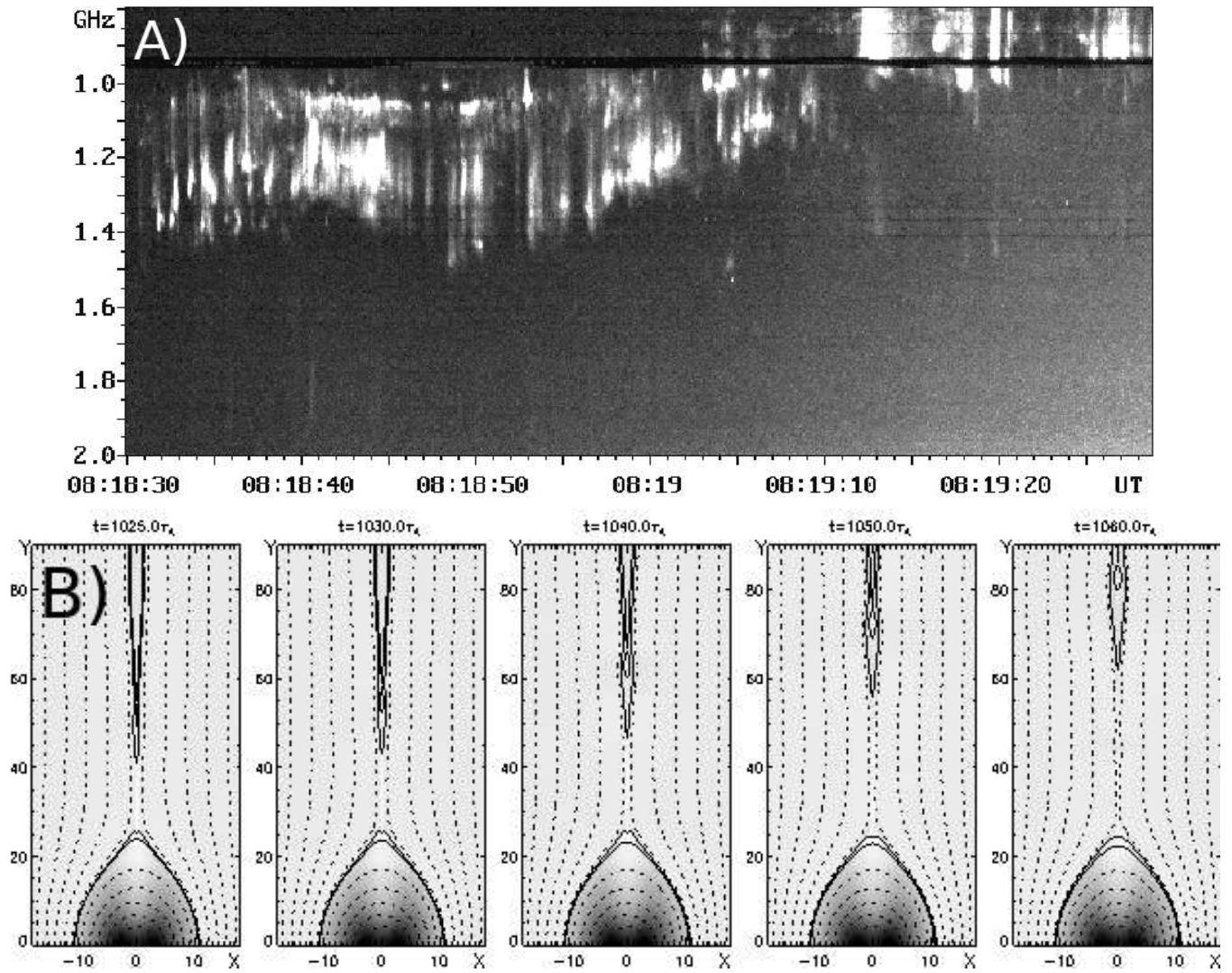


Figure 6. A) Radio spectrum of the 18 August 1998 flare observed by the Ondřejov radiospectrograph showing the drifting pulsation structure (DPS). B) Results of numerical simulations showing formation of the plasmoid that moves upwards in the solar atmosphere, see [Bárta et al. \(2008b\)](#).

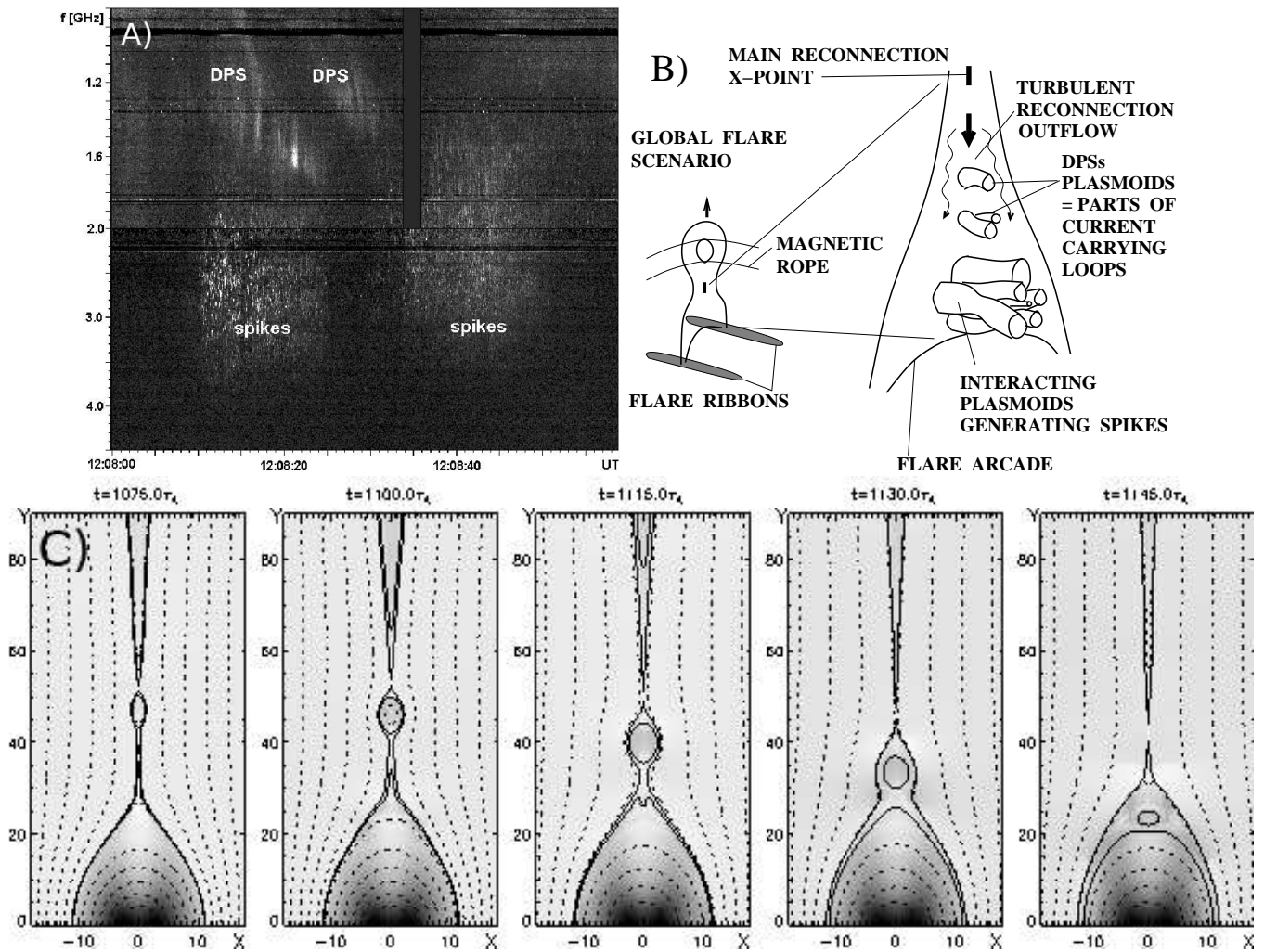


Figure 7. A) Radio spectrum of the 28 March 2001 flare observed by the Ondřejov radiospectrographs showing two DPSs which drift towards the narrowband dm-spikes. B) Scenario of DPSs and dm-spikes generation. C) Results of numerical simulations showing formation of the plasmoid that moves downwards in the solar atmosphere and interacts with the flare arcade, see Bárta et al. (2008b).

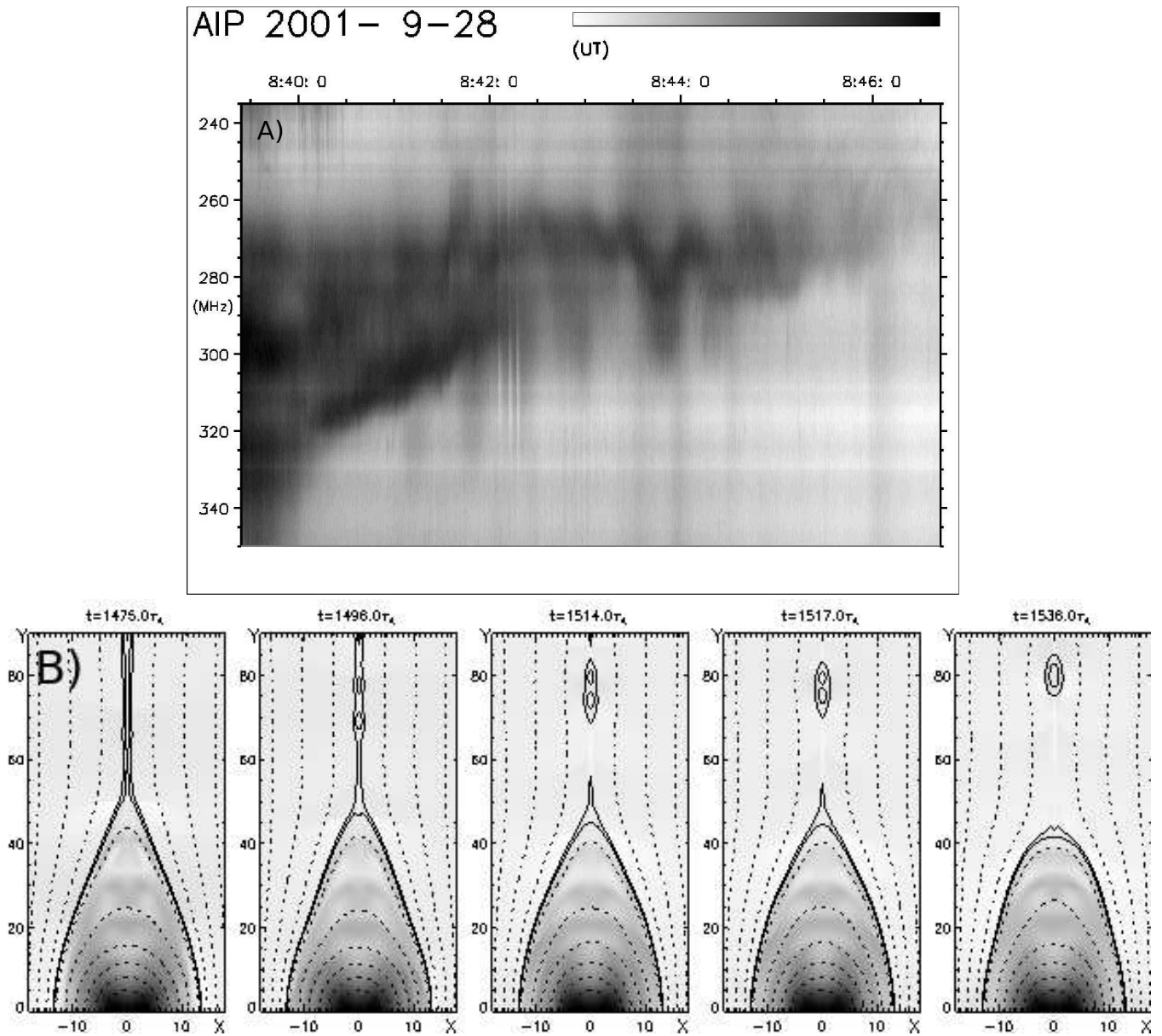


Figure 8. A) Radio spectrum of the 28 September 2001 flare observed by the Potsdam-Tremsdorf radiospectrograph showing two DPSs (08:40 - 08:42 UT) that change into one frequency-varying DPS (after 08:42 UT). B) Results of numerical simulations showing formation of two plasmoids that merge into one oscillating plasmoid, see [Bárta et al. \(2008b\)](#).

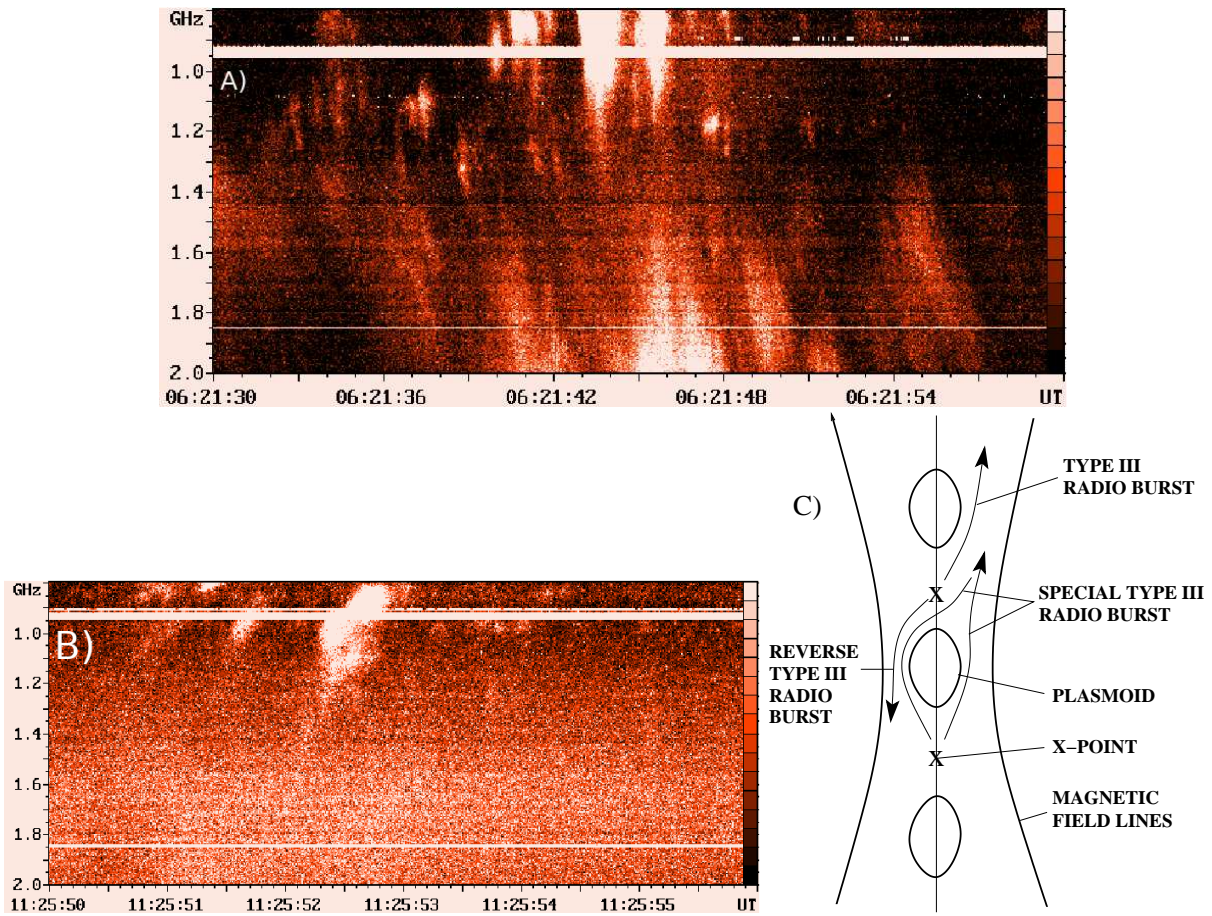


Figure 9. Radio spectra of the 26 September 2011 (A) and 12 February 2010 (B) flares observed by the by the Ondřejov radiospectrograph. The first one shows pairs of normal and reverse drifting decimetric type III bursts and the second shows an unusual decimetric type III burst. C) Scenario for the both bursts explaining them by electron beams.

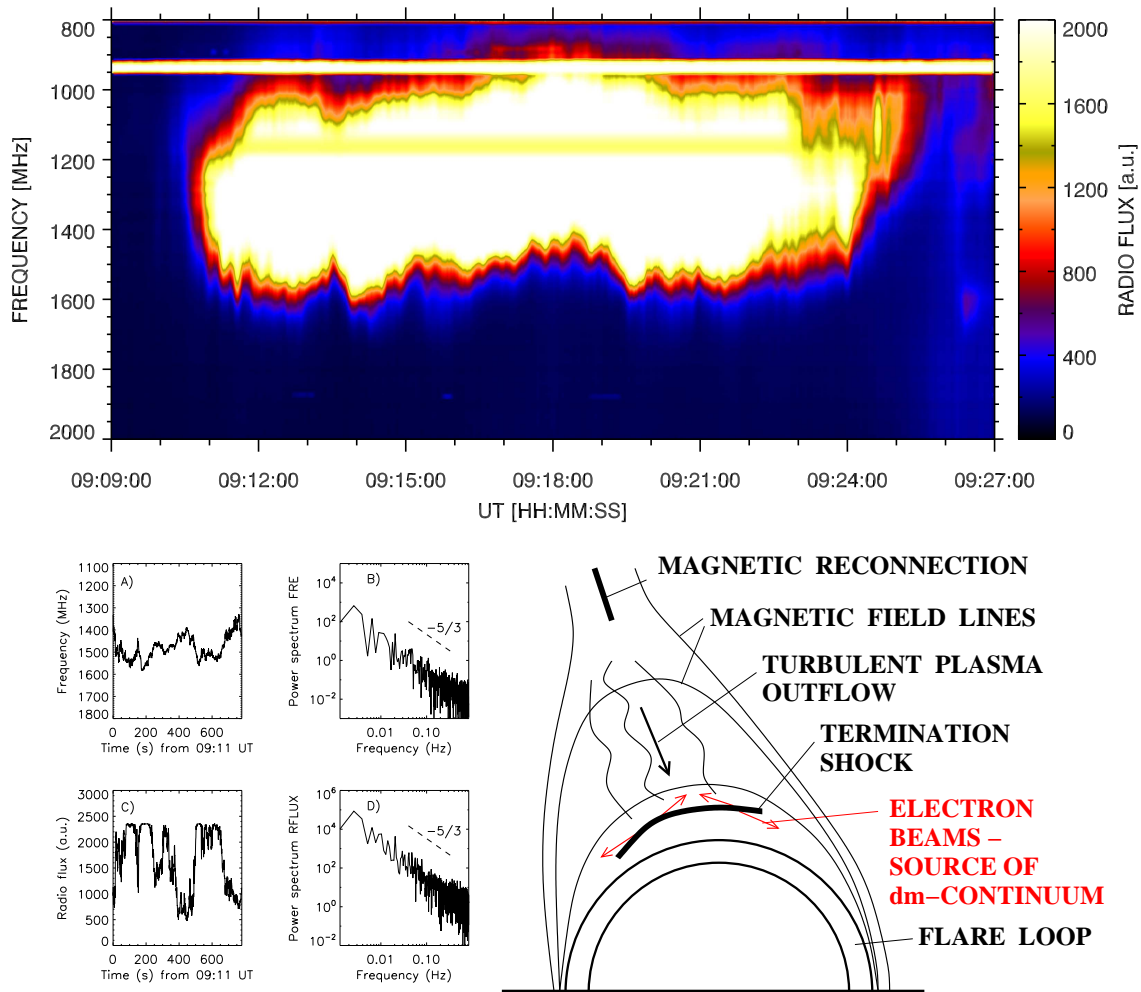


Figure 10. Decimetric continuum observed during the later phase of the 25 June 2015 flare, power spectra (B and D) of frequency variations of the high-frequency continuum boundary (A) and radio flux at 1478 MHz (C) in the 09:11-09:24 UT time interval, and the decimetric continuum model.

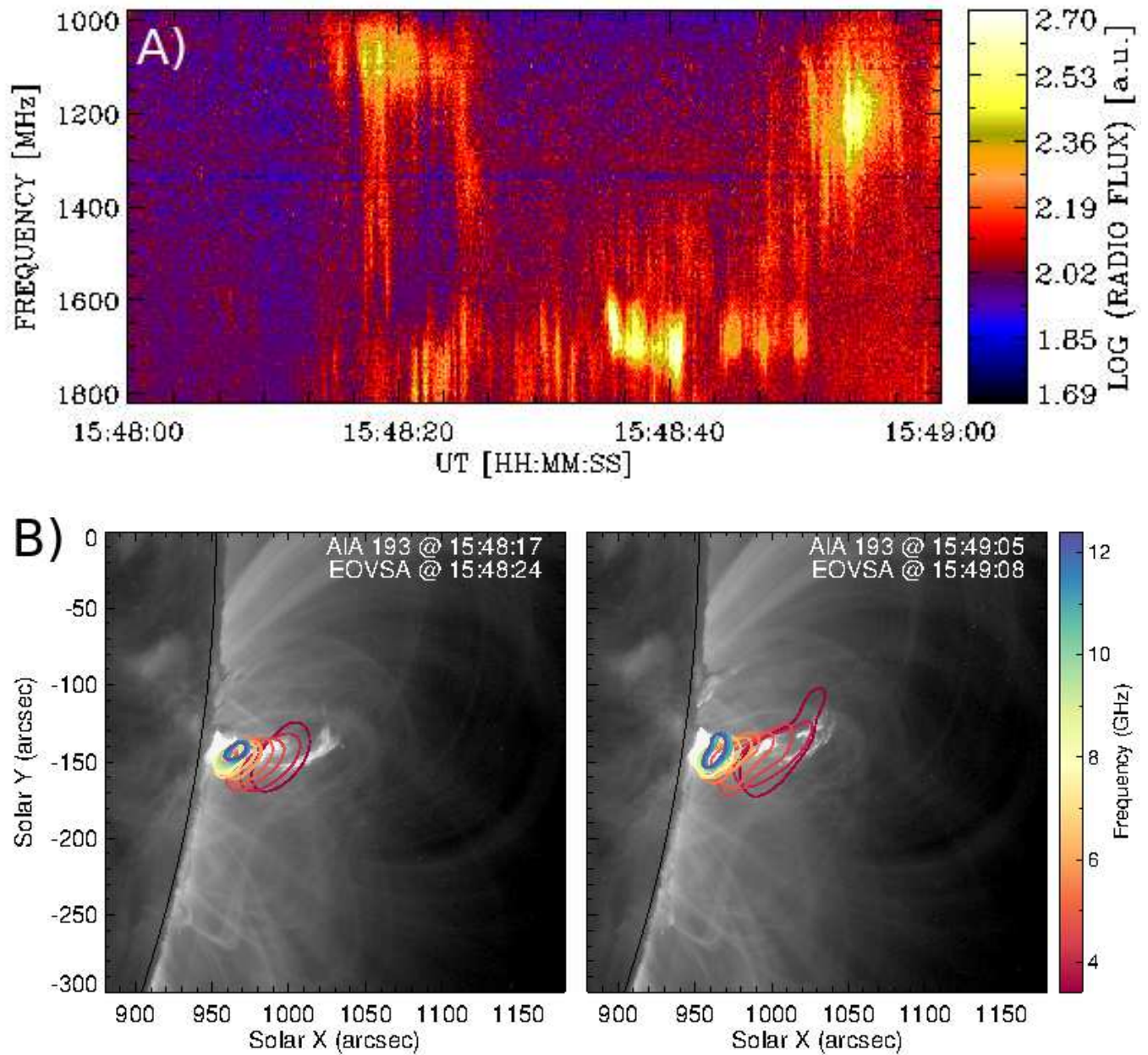


Figure 11. A) Radio spectrum in the 1000-1800 MHz range observed by the Ondřejov radiospectrograph at the very beginning of the 10 September 2017 flare at 15:48-15:49 UT showing DPS with two branches at 1000-1300 MHz and 1500-1800 MHz. B) The EOVSA sources (contours) at 15:48:24 and 15:49:08 UT superimposed on SDO/AIA 193 images in the region of a tearing of the ejected filament.

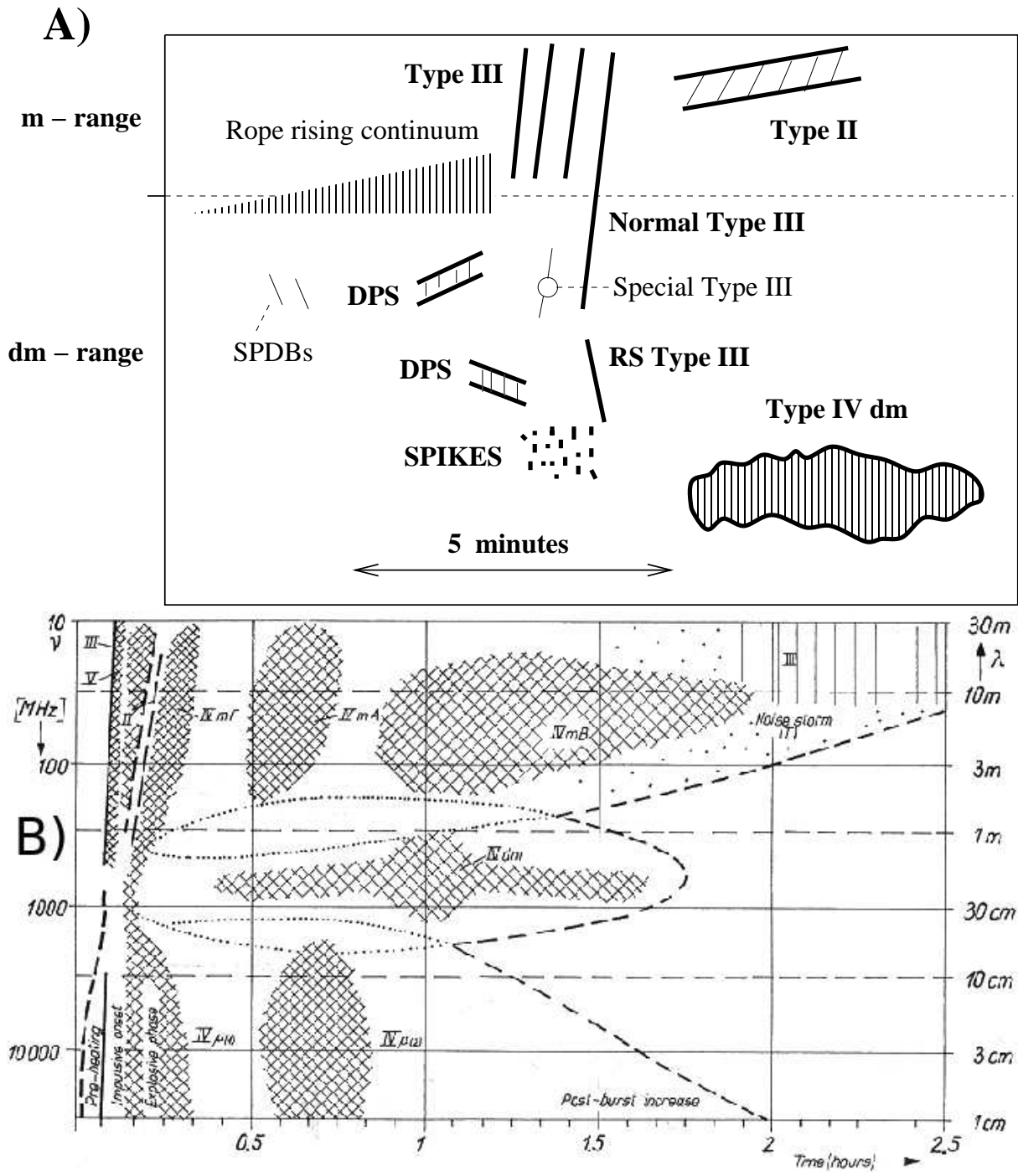


Figure 12. A) Schematic summary of radio bursts observed at the beginning of eruptive flares. The bursts described by thin fonts are very rare. B) Standard schema of radio bursts in solar flares according to [Krueger \(1979\)](#).